In Situ TEM Observation of MgO Nanorod Growth

Albert G. Nasibulin,*,[†] Litao Sun,[‡] Sampsa Hämäläinen,[†] Sergey D. Shandakov,[†,⊥]
Florian Banhart,[‖] and Esko I. Kauppinen[†,#]

[†]NanoMaterials Group, Department of Applied Physics and Center of New Materials,
Helsinki University of Technology, Puumiehenkuja 2, 02150, Espoo, Finland, [‡]Key Laboratory of
MEMS of Ministry of Education, Southeast University, Sipailou 2, Nanjing 210096, China, [‖]Institut de
Physique et Chimie des Matériaux, 23 rue du Loess, Université de Strasbourg, 67034 Strasbourg, France,
[⊥]Laboratory of Carbon NanoMaterials, Department of Physics, Kemerovo State University,
Kemerovo 650043, Russia, and [#]VTT Biotechnology, Biologinkuja 7, 02044, Espoo, Finland

ABSTRACT: The controlled growth of MgO nanorods was investigated under electron irradiation in transmission electron microscopes at accelerating voltages from 120 to 300 kV in the temperature range from −175 to 610 °C. The nanorod growth on the surface of MgO crystals was induced by Au, Pt, Ni, or Co particles of 2−4 nm in size. The nanorods were grown up to 8 nm after 5−30 min of electron irradiation time with beam current densities of 100−600 A/cm^2. The mechanism of nanorod formation and growth is explained on the basis of electrostatic interactions between positive ions of MgO species and negatively charged metal particles.

Quasi one-dimensional nanometer-sized structures have recently attracted significant attention due to their unique properties and wide potential applications in electronic and optic devices, in highly sensitive biological and gas sensors, in catalysis, *etc*.[1−3] Up to now, much attention has been paid to various oxide nanowires and nanorods, which exhibit a rich variety of physical properties, including ferromagnetism, ferroelectric properties, and superconductivity, and might add further functionalities to devices based on quasi one-dimensional nanostructures. Magnesium oxide, a typical wide-band gap insulator, has been extensively used as an additive in refractory experiments due to its high thermal stability, as a paint product, and as a component in high temperature superconductors.[4] MgO has been utilized as a protective film for plasma display screens and included in brake linings, owing to its favorable thermomechanical properties. Extruded magnesia has been applied as a protective sheath in aggressive environments.

MgO crystals were widely used as single crystal substrates for thin film growth due to the small mismatch in lattice parameters with many metals and metal oxides. MgO nanoparticles are typically smooth cubic crystals that are transparent to the electron beam in a transmission electron microscope (TEM) and thereby have been utilized as a substrate for high resolution TEM investigations of particles and clusters.[5−10] During TEM investigations of the most stable Au particle shape on the surface of MgO crystals, Ajayan and Marks noticed the effect of decoupling of the particles from the substrate attributed to the increase in the particle/substrate interfacial energy.[5−7] Giorgio examined the formation of MgO terraces during studies of electron-beam-induced transformation of gold particles.[11] Kizuka observed the formation and subsequent surface structural evolution of the MgO clusters on the surface of Au particles.[11]

Here, we report for the first time that in addition to CVD[11−15] and pulsed laser deposition[16−18] techniques, quasi one-dimensional nanometer MgO structures can be grown under electron beam irradiation of MgO crystals covered by different metals at temperatures as low as −175 °C. We report the results of *in situ* examination of MgO nanorod formation in a TEM under a wide range of parameters: at accelerating voltages from 120 to 300 kV and at temperatures from −175 C to 610 °C. As a material promoting the growth, we have examined Au, Pt, Ni, Co, and Fe sputtered on the surface of MgO substrates. We present a growth mechanism of MgO rods, which can be explained on the basis of electrostatic interactions between metal particles and a substrate.

Cubic MgO nanoparticles were synthesized by burning 5−10 mm sized Mg granules at ambient conditions.[19] The combustion product was collected by passing a carbon-coated copper TEM grid through the smoke about 2−3 cm above the burning granule. Electron diffraction patterns (EDPs), energy dispersive X-ray spectroscopy (EDX), and powder XRD analyses confirmed the formation of MgO (Supporting Information, Figure S1). The existence of $Mg(OH)_2$, $MgCO_3$, and Mg_3N_2, which can be formed due to reaction with water vapor, carbon dioxide, and nitrogen, can be ruled out. Statistical measurements of MgO particles from TEM images revealed the log−normal particle size distribution with the geometric mean diameter of 37.7 nm and the standard deviation of 1.91 (Supporting Information, Figure S2). Au, Pt, Ni, Co, or Fe were sputtered on TEM grids with predeposited MgO particles using an Agar sputter coater (model 108A) under 0.05 mbar of Ar pressure at 20 mA dc at the distance from the metal target of 37 mm. Sputtering time was varied from 5 to 25 s.

Electron irradiation and imaging were carried out in three different microscopes (FEI Tecnai F-30, Philips CM-200 and CM12) with an acceleration voltage ranging from 120 to 300 kV. A heating stage (Philips) and a cooling stage (Gatan) were used to keep the specimens at different temperatures during the irradiation experiments. Selected MgO particles were subjected to intense electron irradiation with beam current densities of 100−600 A/cm^2 and monitored *in situ* with high resolution by taking images in certain time intervals.

*To whom all correspondence should be addressed: Telephone: +358 50 3397538. Fax: +358 451 3517. E-mail: albert.nasibulin@hut.fi.
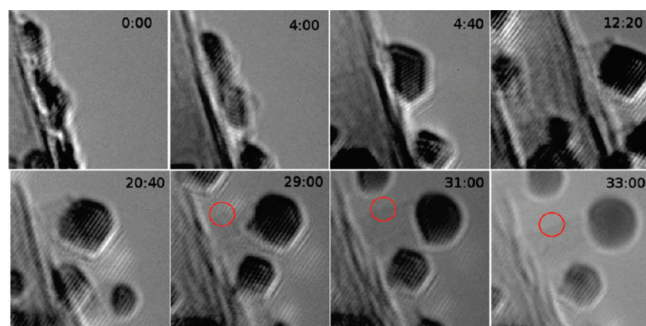
Figure 1. Growth of MgO nanorods in a TEM at room temperature (200 kV). The time from the start of the irradiation is displayed on each image (in min:sec). As can be seen, diffusion of Pt on the surface (first 3 images) occurred much more quickly than the actual growth. Beam current density: 200 A/cm². Each image represents an area of 9.2×9.2 nm². The red circles show the edge of a MgO nanorod.

For MgO nanorod growth, we applied Pt, Au, Ni, and Co. However, Fe sputtered on the surface of MgO particles did not result in the growth of nanorods (Supporting Information, Figures S4−S6). The statistical measurements of the diameters of MgO nanorods grown using Pt and Au particles revealed that nanorods had mean diameters of 2.2 and 2.4 nm, respectively (Supporting Information, Figure S3). As an example, Figure 1 shows the formation of MgO nanorods under an electron beam growing from Pt particles on the surface of cubic MgO particles at room temperature with the accelerating voltage of 200 kV and current density of approximately 200 A/cm². A capped MgO nanorod is seen to start growing from the Pt particle after irradiation for 12 min. The MgO nanorod keeps growing as the irradiation continues. Depending on the intensity of the electron beam, the growth of nanorods was observed after a 5−30 min irradiation time. Metal particles on the surface of MgO induced the growth of MgO nanorods with the maximum length of 8 nm.

It is worth noting that there is an epitaxial relationship between MgO and metal particles. Moreover, the nanorods grow only in the direction family of ⟨200⟩. No influence of the electron beam direction on the direction of the nanorods was found. Figure 2 shows the starting moment of the MgO nanorod growth. Before nanorod growth, the lattices of Pt particles become aligned according to the MgO substrate. The process of nanorod growth starts only after the rearrangement of the metal particles on the substrate. The epitaxial relationship is preserved during the nanorod growth, as can be seen in Figure 3. The nanorod growth termination is usually associated with the fact that metal particles lose their crystallographic features and as a result their epitaxial relationship with MgO nanorods and take the spherical form.

The mechanism of the nanorod formation can be explained on the basis of an electrostatic repulsion−attraction mechanism. Under electron beam irradiation, MgO particles are charged positively.[12] The process of charging is related to a high secondary electron emission coefficient of MgO[20] and Auger electron emission.[21] In addition to positive ions of Mg and MgO molecules, O^+ emerges according to the Auger process based on the Knotek−Feibelman mechanism.[12] The secondary electron emission yield for metals, however, is < 1 at high energies.[21] Also, there is a probability of metal particles to be negatively charged by trapping secondary electrons emitted from MgO particles. Therefore, MgO particles are charged positively whereas the metal particles might possess negative charges (Figure 4).
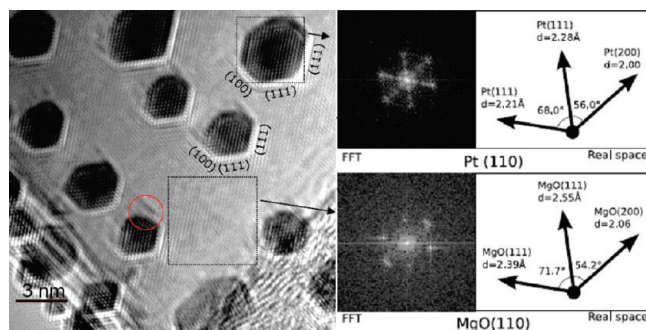

Figure 2. Facets of the Pt particles when the MgO nanorod growth is just initiated. The image views both lattices in the (110) direction. The red circle shows the edge of a MgO nanorod. It is worth noting that the lattices of the Pt particles and the MgO cube are aligned.
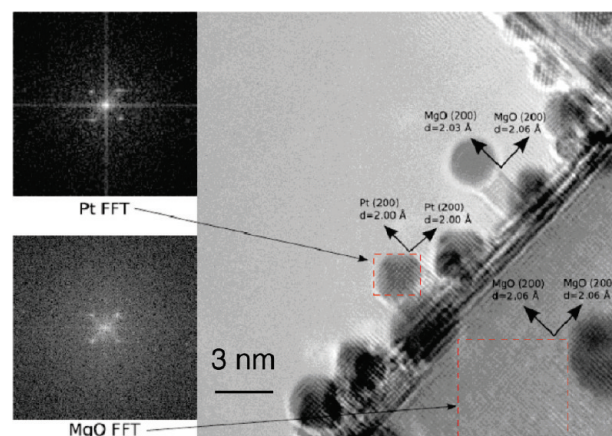

Figure 3. Lattice constants and orientations of the Pt particles and MgO crystals and nanorods indicating their epitaxial relationship. The image views both lattices in the (100) direction. The lattices of the MgO block and Pt particle were calculated from the Fourier transforms depicted on the left. The lattice constants of the MgO nanorod were measured directly from the image.

Under the electron beam irradiation, diffusion of MgO species (O^+, MgO^+, and Mg^+) on the surface of a MgO crystal is relatively high.[12] These ions can be attracted by negatively charged metal particles and trapped at the boundary between the particle and the MgO. Here, the ions are discharged by the excessive electrons on the metal and start to build a crystallographic lattice epitaxially underneath the metal particle. The nanorod growth starts after some delay, as we observed, which is most likely due to the creation of the interface between the growing nanorod and the metal particle. It is worth noting that the charging and discharging processes are dynamic processes: the metal particle can be charged by trapping low energy secondary electrons emitted from MgO particles and can be discharged due to the interaction with positively charged ions. The rate of charging and discharging of a metal particle determines the rate of the nanorod growth. After the nanorod growth is initiated, there are two possible scenarios depending on the irradiation intensity. At high growth rates, the bottom of the metal particle is encapsulated inside the growing nanorod as shown in Figure 5, where a part of the Au particle detaches and gets trapped. At slow growth rates, the metal particle always remains on the top of the nanorod. The nanorod growth can be observed in a certain range of the beam intensities. The best growth conditions were obtained at the beam current density from 200 to 300 A/cm².
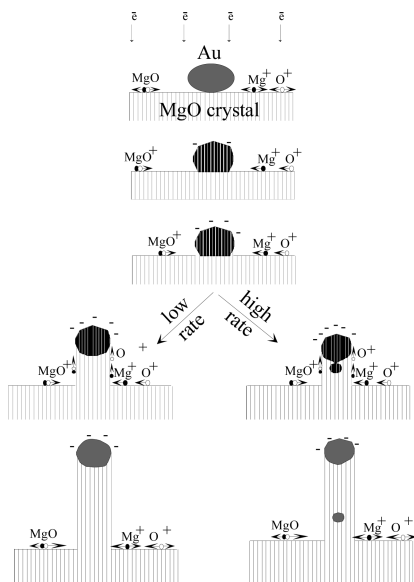
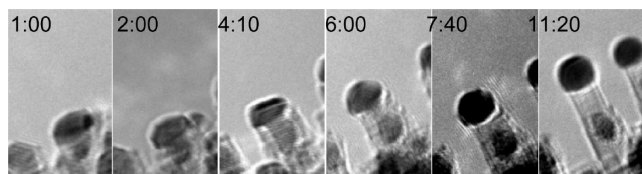**Figure 4.** Proposed mechanism of MgO rod growth at low or high growth rate.

Figure 5. Growth of MgO nanorods by Au particles at room temperature. Part of the Au particle detaches and gets trapped inside the rod. Beam current density: around 200 A/cm^2. Each image represents an area of 9.4×15.0 nm^2 (Supporting Information, movie 1). The time from the start of the irradiation is displayed on each image (in min:sec).

Let us discuss the reason for termination of the nanorod growth when the length reaches 6–8 nm. The Coulombic attraction between metal particle and ions on the crystal surface becomes weaker when the nanorod length increases and therefore the flux of building ions (O$^+$, MgO$^+$, and Mg$^+$) to the particles decreases. As a result, the nanorod growth is suppressed and the metal particle accumulates negative charges. This can lead to attraction of the metal to the positively charged MgO particle. Indeed, Au and Pt particles were observed to fall from the tip of the nanorod to the MgO particle and induce the growth of another nanorod, while the previously grown nanorod continuously disappears (Figure 6 and Supporting Information, movie S1). The termination of the nanorod growth was also observed due to the Ostwald ripening effect,[22] when small particles vanish from the surface and even from the tip of the nanorods, while large particles become larger (Supporting Information, Figure S7 and movie S2).

In order to verify the importance of charging phenomena, we carried out experiments where the charging effect was partially suppressed. For this purpose, we irradiated MgO particles sitting close to the edge of a copper grid. In this arrangement, the charging of MgO can be suppressed because secondary electron emission from the massive grid discharges the MgO nanoparticles. This is a common technique to avoid charging of insulators in the electron beam of a TEM. Indeed, no nanorod growth was observed close to the copper grid,
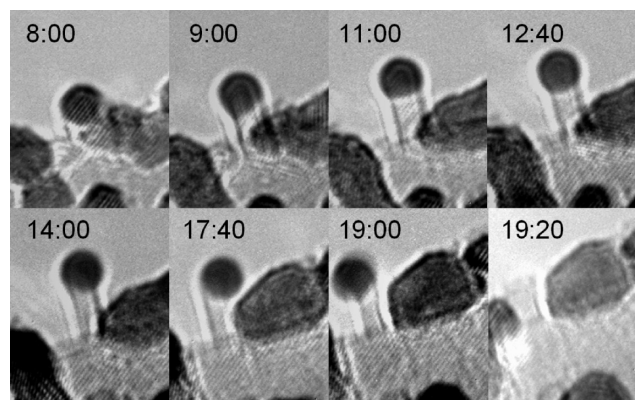

Figure 6. Growth of a MgO nanorod catalyzed by a Pt particle and termination due to the loss of the catalyst at room temperature (200 kV). Each image represents an area of 9.2×11.5 nm^2. The time from the start of the irradiation is displayed on each image (in min:sec).
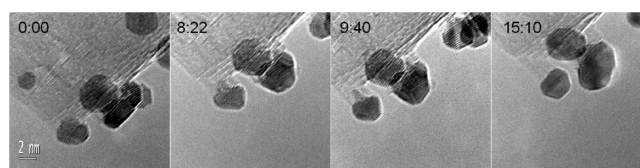

Figure 7. Growth of MgO nanorods by Au particles under electron irradiation at -175 °C (300 kV). Beam current density: 300 A/cm^2. Each image represents an area of 9.2×9.2 nm^2. The time from the start of the irradiation is displayed on each image (in min:sec).

confirming the electrical nature of the nanorod growth (Supporting Information, Figure S8).

It is important to note that Fe sputtered on the surface of MgO did not result in the growth of nanorods (Supporting Information, Figure S6). This can be explained by formation of iron oxide after taking the substrate with sputtered Fe to the ambient conditions. Iron oxide particles on the surface of the MgO crystal would not initiate the nanorod growth.

According to a possible thermal nature of MgO nanorod growth, it is worth noting that the growth was observed in the temperature range from -175 to 300 °C. At higher temperatures, due to higher diffusion of atoms and small particles on the surface of MgO, the nanorod growth was suppressed by the enhanced Ostwald ripening effect (Supporting Information, Figure S9). Metal particles with excessive size were not observed to induce the growth of nanorods. TEM observations showed that the particles shrink due to surface diffusion and finally disappear under long-time irradiation at 610 °C (Supporting Information, Figure S10). TEM images illustrating the growth of MgO nanorods at -175 °C are shown in Figure 7. It is worth noting that this is the lowest temperature at which nanorods have been synthesized. The process of nanorod growth at this temperature is more stable (no drift or vibrating during the irradiation) than that at room temperature, and the growth rate seemed to be faster. Therefore, the growth of nanorods is not directly associated with the thermal energy. A considerable heating of these objects in the electron beam can be neglected due to the low contribution of inelastic scattering.

In conclusion, we investigated the growth of MgO nanorods under electron irradiation of MgO covered by 2–4 nm sized Au, Pt, Ni, or Co particles. Growth of MgO nanorods was found at accelerating voltages from 120 to 300 kV and in

the temperature range from −175 to 300 °C. At higher temperatures, the growth of nanorods was suppressed by overgrowth of metal particles due to the Ostwald ripening effect. Termination of MgO nanorod growth was found to occur due to the loss of metal particles. Fe did not result in the growth of nanorods due to the formation of iron oxide on the surface of a MgO crystal. The nanorod growth was explained on the basis of an electrostatic repulsion−attraction interaction mechanism.

Supporting Information Available: (1) Characterization of MgO particles; (2) statistical measurements; (3) Co, Ni, and Fe as a catalyst; (4) Ostwald ripening effect; (5) nanorod growth near a copper grid; (6) electron irradiation at high temperatures; and (7) movies. This information is available free of charge via the Internet at http://pubs.acs.org/.

References

(1) Patolsky, F.; Timko, B. D.; Yu, G.; Fang, Y.; Greytak, A. B.; Zheng, G.; Lieber, C. M. *Science* **2006**, *313*, 1100–1104.

(2) Xiang, J.; Lu, W.; Hu, Y.; Wu, Y.; Yan, H.; Lieber, C. M. *Nature* **2006**, *441*, 489–493.

(3) Li, Y.; Qian, F.; Xiang, J.; Lieber, C. M. *Mater. Today* **2006**, *9*, 18–27.

(4) Zhao, M.; Chen, X. L.; Wang, W. J.; Ma, Y. J.; Xu, Y. P.; Zhao, H. Z. *Mater. Lett.* **2006**, *60*, 2017–2019.

(5) Ajayan, P. M.; Marks, L. D. *Phys. Rev. Lett.* **1989**, *63*, 279–282.

(6) Ajayan, P. M.; Marks, L. D. *Nature* **1989**, *338*, 139–141.

(7) Ajayan, P. M.; Iijima, S. J. *Colloid Interface Sci.* **1991**, *147*, 281–285.

(8) Shashkov, D. A.; Chisholm, M. F.; Seidman, D. N. *Acta Mater.* **1999**, *47*, 3939–3951.

(9) Wang, C. M.; Shutthanandan, V.; Zhang, Y.; Thevuthasan, S.; Duscher, G. *JASC* **2005**, *88*, 3184–3191.

(10) Hoel, R. H. *Surf. Sci.* **1986**, *169*, 317–326.

(11) Giorgio, S.; Henry, C. R.; Chapon, C.; Nihoul, G.; Penisson, J. M. *Utramicroscopy* **1991**, *38*, 1–12.

(12) Kizuka, T. *Jpn. J. Appl. Phys.* **2001**, *40*, L1061–L1064.

(13) Chen, Y.; Li, J.; Han, Y.; Yang, X.; Dai, J. *J. Cryst. Growth* **2002**, *245*, 163−170.

(14) Yang, Q.; Sha, J.; Wang, L.; Wang, J.; Yang, D. *Mater. Sci. Eng. C* **2006**, *26*, 1097–1101.

(15) Kim, H. W.; Shim, S. H. *Chem. Phys. Lett.* **2006**, *422*, 165–169.

(16) Nagashima, K.; Yanagida, T.; Tanaka, H.; Kawai, T. *J. Appl. Phys.* **2007**, *101*, 124304.

(17) Nagashima, K.; Yanagida, T.; Tanaka, H.; Kawai, T. *Appl. Phys. Lett.* **2007**, *90*, 233103.

(18) Marcu, A.; Yanagida, T.; Nagashima; Tanaka, H.; Kawai, T. *J. Appl. Phys.* **2007**, *102*, 016102.

(19) Altman, I. S.; Pikhitsa, P. V.; Choi, M.; Nasibulin, A. G.; Kauppinen, E. I. *Phys. Rev. B* **2003**, *68*, 125324.

(20) Whetten, N. R.; Laponsky, A. B. *J. Appl. Phys.* **1958**, *30*, 432–435.

(21) Williams, D. B.; Carter, C. B. *Transmission Electron Microscopy—Basics*; Plenum Press: New York, London, 1996.

(22) Hannon, J. B.; Kodambaka, S.; Ross, F. M.; Tromp, R. M. *Nature* **2006**, 69–71.